Microporous and Mesoporous Materials 270 (2018) 265–273

Contents lists available at ScienceDirect

Microporous and Mesoporous Materials

journal homepage: www.elsevier.com/locate/micromeso

Facile synthesis of Sn-containing MFI zeolites as versatile solid acid catalysts

Enhui Yuan[a], Weili Dai[a,*], Guangjun Wu[a,b], Naijia Guan[a,b], Michael Hunger[c], Landong Li[a,b,**]

[a] School of Materials Science and Engineering & National Institute for Advanced Materials, Nankai University, Tianjin, 300350, PR China
[b] Key Laboratory of Advanced Energy Materials Chemistry of Ministry of Education, Collaborative Innovation Center of Chemical Science and Engineering, Nankai University, Tianjin, 300071, PR China
[c] Institute of Chemical Technology, University of Stuttgart, 70550 Stuttgart, Germany

ARTICLE INFO

Keywords:
Sn-MFI
EDTA-Sn
Lewis acid catalysis
Dihydroxyacetone
Methyl lactate

ABSTRACT

Sn-containing MFI zeolites with controllable Al contents were successfully synthesized with the utilization of the EDTA-Sn complex as tin source and citrate as buffer solution for the first time. The elaborately strategy achieves a right release of Sn^{4+} ions rate to combine with the silicon tetrahedron species in the synthesis process which could make the heteroatom tin warmly incorporate into the zeolite frameworks. The structural information about the Sn-containing MFI zeolites was confirmed by XRD, FTIR, and solid-state NMR spectroscopy. Characterization results of HRTEM, FTIR, XPS, and UV-vis spectroscopy illustrated that most Sn species exist as isolated tetrahedral Sn(IV) in the as-prepared zeolites. The creation of Lewis acid sites in Sn-MFI and Sn-Al-MFI zeolites, and Brønsted acid sites in Sn-Al-MFI zeolites were determined by FTIR spectroscopy of pyridine adsorption and ^{1}H and ^{31}P MAS NMR spectroscopy after ammonia and trimethylphosphine oxide (TMPO) adsorption. Both the Sn-MFI and Sn-Al-MFI zeolite catalysts exhibit a remarkable catalytic performance in the conversion of dihydroxyacetone (DHA) to methyl lactate (ML), while the bifunctional Sn-Al-MFI catalyst exhibits a significant combination effect, and a remarkable active site-based turnover frequency with a high methyl lactate productivity can be achieved.

1. Introduction

The heteroatoms substituted zeolites have been widely employed in heterogeneously catalyzed processes due to their distinct pore dimension, interconnectivity, and compositions [1–5]. The microporous crystalline frameworks of most zeolites possess high hydrothermal stability and feature attractive shape and transition-state selectivity effects. On the other side, the incorporated heteroatoms can also endow other specific properties for the zeolites, e.g. redox activity and Lewis acidity [6–9]. These representative properties of the heteroatoms substituted zeolites make it is possible to employ them in many important reactions.

As a sustainable process for production of high-value products from renewable biomass-derived compounds, the conversion of triose sugars to lactic acid and alkyl lactates has attracted significant attention recently [10–12]. The reaction processes include two main steps, i.e. dehydration and rearrangement, which can be catalyzed by weak Brønsted acid sites and strong Lewis acid sites, respectively [13–18]. The Sn-containing Lewis acidic zeolites, e.g. Sn-BEA and Sn-MFI, has been proved to be active in this reaction [19–22]. In addition, the combination of Lewis and Brønsted acid sites in Sn-containing zeolites can greatly promote their catalytic activity, because Brønsted acidity facilitates the rate-determining dehydration of dihydroxyacetone (DHA) [14]. Therefore, the bifunctional Sn-containing zeolites with the controllable Lewis and Brønsted acid sites are mostly desired for this reaction.

For the preparation of Sn-containing zeolites, e.g. Sn-Beta, both direct hydrothermal synthesis and post-synthesis modification strategies have been reported. The traditional hydrothermal synthesis of Sn-BEA, usually requires a long crystallization time, and the participation of the noxious fluoride as mineralizing agent [19]. On the other hand, the post-synthesis modification strategy involves concentrated nitric acid in a large amount to dealuminate the parent zeolite and the obtained materials highly depend on the detailed procedures of Sn incorporation [20,21]. In comparison with Sn-Beta, the direct synthesis of Sn-MFI is relative easy, but a long crystallization time of 6–7 days is also required when fluoride is utilized as mineralizing agent [8,22]. In this context, a facile fluoride-free strategy to directly synthesize Sn-containing zeolites within a short crystallization time is urgent. Recently, several fluoride-free routes to synthesize Sn-MFI zeolites with

* Corresponding author.
** Corresponding author. School of Materials Science and Engineering & National Institute for Advanced Materials, Nankai University, Tianjin, 300350, PR China.
E-mail addresses: weilidai@nankai.edu.cn (W. Dai), lild@nankai.edu.cn (L. Li).

https://doi.org/10.1016/j.micromeso.2018.05.032
Received 26 March 2018; Received in revised form 11 May 2018; Accepted 21 May 2018
Available online 23 May 2018
1387-1811/

the direct addition of $SnCl_4$ into the synthesis systems have been reported [22–24], but the Sn species cannot be fully integrated into the structure because the fast hydrolysis and precipitation of $SnCl_4$ in the alkaline environments [23,24]. Additionally, the pH values of the synthesis solution greatly decrease because of the strong hydrolysis of $SnCl_4$ [25,26], which can lead the silicon species rapidly condense and make the seriflux agglutinated and hard to stir [23]. That is, a lack of productivity and reproducibility might be encountered in actual operation of fluoride-free synthesize Sn-containing zeolites. In this context, a facile strategy to directly synthesize Sn-MFI zeolite with the homogeneous distribution of tetra-coordinated Sn(IV) species is urgently desired. For its application in the typical reaction, e.g. dihydroxy-acetone (DHA) to methyl lactate (ML) conversion, facile synthesis of the bifunctional Sn-containing MFI zeolites with the controllable Lewis acidic Sn (IV) sites and the Brønsted acidic Al(III) sites is mostly desired, and is, therefore, the aim of this work.

In this work, we report a facile strategy for the direct hydrothermal synthesis of nano-sized Sn-containing MFI zeolites with controllable Al contents. The incorporation of Sn species into MFI zeolites is accomplished by using ethylenediaminetetraacetic acid tin salt (EDTA-Sn) as the Sn source and a sodium citrate buffer solution to suppress the hydrolysis of the tin salt during the synthesis process. The structural information about the Sn-containing MFI zeolites was confirmed by XRD, FTIR, and solid-state NMR spectroscopy. The existing states and distribution of Sn species in the Sn-containing MFI zeolites were investigated by FTIR, XPS, UV-vis spectroscopy, and HRTEM microscopy. The creation of Lewis acid sites in Sn-MFI and Sn-Al-MFI zeolites, and Brønsted acid sites in Sn-Al-MFI zeolites, were determined by FTIR spectroscopy of pyridine adsorption and 1H and 31P MAS NMR spectroscopy after ammonia and TMPO adsorption. Both Al-free Sn-MFI and Al-containing Sn-Al-MFI materials under study exhibit remarkable catalytic activities in the conversion of DHA to ML, while a beneficial combination effect between Lewis acidic Sn sites and Brønsted acidic Si(OH)Al groups was achieved with Sn-Al-MFI.

2. Experimental sections

2.1. Zeolite synthesis

2.1.1. Synthesis of Sn-MFI zeolites

An in situ hydrothermal route was employed for the synthesis of Sn-MFI zeolites (Scheme S1). In a typical experiment, 0.40 g NaOH, 17.40 g tetrapropylammonium hydroxide (25% TPAOH) and 5.20 g fumed silicon were first mixed with 15.0 mL H_2O and stirred at 60 °C for 6 h, which was denoted as **solution A**. Second, 0.50 g EDTA-2Na (ethylenediaminetetraacetic acid disodium salt hydrate) and 0.78 g sodium citrate dehydrate were added into 10.0 mL H_2O under stirring at 60 °C. Thereafter, the mixed liquor of 0.46 g stannic chloride pentahydrate and 5.0 mL H_2O were added into the mixture drop by drop, then a certain amount of Na_2CO_3 were added to neutralize the solution, which was denoted as **solution B**. Third, **solution B** was dropwise added into the **solution A** under stirring at 60 °C for 3 h and transferred into a Teflon-lined autoclave and heated at 200 °C for 72 h. The solid product was recovered by centrifugation, washed to neutral with deionized water and dried at 80 °C. The structure-directing agent was removed from the product by calcination at 550 °C in flowing air for 6 h. The calcined product was treated in 5% NH_4Cl aqueous solution at 80 °C for 4 h, filtrated, thoroughly washed and dried. The final product was obtained by calcination of the above-mentioned sample at 550 °C in flowing air for 6 h. With different tin content, the molar composition of the batch was controlled as SiO_2/(0.01–0.02) SnO_2/(0.01–0.02) EDTA-2Na/0.06 Na_2O/0.25 TPAOH/28 H_2O, and the final products were labelled as wt.% Sn-MFI, where wt. represents the actual Sn loading in the sample.

The addition of a certain amount of sodium citrate dehydrate into the EDTA-2Na solution in the second step is to inhibit the precipitation of EDTA-4H upon the introduction of $SnCl_4$ because the intensive hydrolysis of $SnCl_4$ would make a strong acidic solution and the solubility of EDTA-4H in an acid system is very low. The sodium citrate dehydrate here act as a buffer reagent. Simultaneously, the goal of adding a certain amount of Na_2CO_3 solid skillfully into the buffer solution is to expend the H^+ that come from the hydrolysis of $SnCl_4$ before the complexes mixtures put into the synthesis gel. Adding this markedly neutral tin complexes solution directly into the synthesis systems, which achieves a right release rate of Sn^{4+} ions to combine with the silicon tetrahedron species through fine coordination bonding interactions between the tin ions and ethylene diamine tetra acetic groups. After a period of crystallization process, these tin ions can be successfully incorporated into the zeolite frameworks.

2.1.2. Synthesis of Sn-Al-MFI zeolites

A similar in situ hydrothermal route was employed for the synthesis of Sn-Al-MFI zeolites, and a certain amount aluminum sulfate was added together with fumed silicon. The molar composition of the batch was controlled as SiO_2/(0.006–0.013) Al_2O_3/0.015 SnO_2/0.015 EDTA-2Na/(0.06–0.068) Na_2O/0.25 TPAOH/28 H_2O. The final products were labelled as wt.% Sn-Al-MFI-x, where wt. and x represent the actual Sn loading and Si/Al ratio, respectively.

2.2. Characterization techniques

The X-ray powder diffraction (XRD) patterns of zeolite samples were collected on a Rigaku MiniFlex II instrument with Cu Kα radiation and operating at an acceleration voltage of 35 kV and a current of 30 mA.

The surface areas of Sn-containing zeolites were determined by nitrogen adsorption/desorption isotherms at 77 K collected on a Quantachrome iQ-MP gas adsorption analyzer. The total surface area was calculated via the Brunauer Emmett Teller (BET) equation and the micropore size distribution was determined using the t-plot method.

The exact Si, Al and Sn contents of the zeolites were analyzed by inductively coupled plasma optical emission spectroscopy (ICP-OES, Series X7, Thermo Electron Corporation).

The morphology of selected zeolite sample was observed using a scanning electron microscope (JSM-7500F).

Transmission electron microscopy (TEM) and high-resolution transmission electron microscopy (HRTEM) images were recorded on a JEOL JEM-2100F electron microscope with an acceleration voltage of 200 kV.

Infrared Fourier transform (FTIR) spectra of zeolite samples were taken by a Bruker Tensor 27 spectrometer with 128 scans at a resolution of 2 cm^{-1} against KBr as the background.

Diffuse reflectance ultraviolet-visible (UV-vis) spectra of the dehydrated zeolite samples were measured in the range of 200–1000 nm with a PerkinElmer Lambda 750 UV-Vis-NIR spectrophotometer.

X-ray photoelectron spectra (XPS) of materials were recorded on a Thermo Scientific ESCALAB 250Xi spectrometer with a monochromatic Al-Kα X-ray source ($h\nu$ = 1486.6 eV) as the excitation source. Accurate binding energies (± 0.1 eV) were determined with respect to the position of the adventitious C 1s peak at 284.8 eV.

The temperature-programmed desorption of ammonia (NH_3-TPD) was performed using a Quantachrome ChemBet 3000 chemisorption instrument. In a typical experiment, the sample was saturated with 5% NH_3/He at 50 °C and then purged with He at the same temperature for 1 h to eliminate the physical absorbed ammonia. NH_3-TPD profile was recorded in flowing He at a heating rate of 10 °C/min from 50 to 600 °C.

FTIR spectra of pyridine adsorption were also collected on the Bruker Tensor 27 spectrometer with 128 scans at a resolution of 2 cm^{-1}. A self-supporting pellet made of the sample was placed in a flow cell and evacuated at 400 °C for 4 h. After cooling to room temperature, the samples were saturated with pyridine vapor and then evacuated at 200 °C for 1 h. Spectra were recorded at evacuation temperature in the 2000-1000 cm^{-1} range.

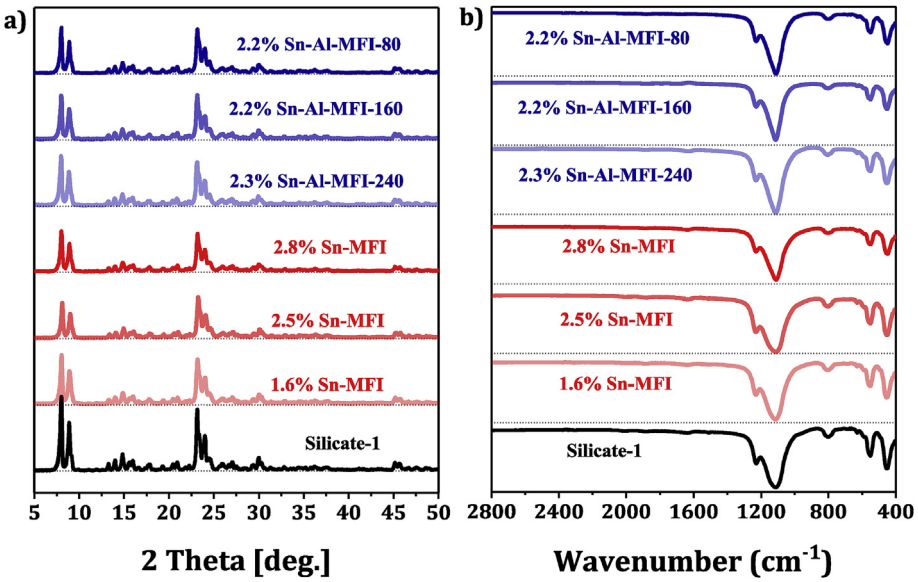

Fig. 1. (a) XRD patterns of Silicate-1 and Sn containing MFI zeolites; (b) FT-IR spectra of Silicate-1 and Sn containing MFI zeolites.

Magic angle spinning nuclear magnetic resonance (MAS NMR) experiments were performed on a Bruker Avance III spectrometer at resonance frequencies of 400.1, 104.3, 79.5 MHz, and 161.9 MHz for ^{1}H, ^{27}Al, ^{29}Si and ^{31}P nuclei, respectively. The experimental conditions are as follows: single pulse π/2 excitation for ^{1}H, ^{29}Si, and ^{31}P, π/6 for ^{27}Al, and repetition times of 20 s for ^{1}H and ^{29}Si, 0.5 s for ^{27}Al, and 30 s for ^{31}P MAS NMR spectroscopy. The ^{1}H, ^{27}Al, and ^{31}P MAS NMR spectra were recorded with a sample spinning rate of 8 kHz (^{1}H, ^{27}Al) and 10 kHz (^{31}P) using 4 mm rotors, while the ^{29}Si MAS NMR spectra were obtained with 4 kHz using 7 mm rotors. All of the ^{1}H and ^{31}P MAS NMR studies were performed using dehydrated samples, which were treated at 450 °C in vacuum (below 10^{-2} Pa) for 12 h. Thereafter, the probe molecules, i.e., ammonia and TMPO, were loaded for further measurements. Loading of the dehydrated catalysts with TMPO (Alfa Aesar) was performed inside a glove box, purged with dry nitrogen gas, by mixing ca. 50 mg of the dehydrated samples with ca. 2.5 mg TMPO inside a rotor, which was subsequently sealed with an O-ring-containing Marcor-Cap. In a further step, the TMPO-loaded samples inside the sealed rotors were heated at 160 °C for 2 h for reaching a homogeneous distribution of the probe molecules on the sample material. The ammonia loading of the dehydrated samples was done on a vacuum line by adsorption of 100 mbar ammonia (Griesinger) at 25 °C for 10 min, followed by an evacuation ($p < 10^{-2}$ mbar) at 180 °C for 2 h for removing weakly physisorbed ammonia. Quantitative ^{1}H MAS NMR measurements were performed by using zeolite 35H,65Na-Y (decationization degree of 35%) as an external intensity standard. ^{1}H MAS NMR difference spectra of the unloaded and ammonia-loaded samples under study were utilized for the signal separation and the determination of the relative signal intensities. For the calculation of the number of NH_4^+ at former Brønsted acid sites and of NH_3 coordinated at Lewis acid sites, the integral intensities of the corresponding ^{1}H MAS NMR signals were divided by 4 and 3, respectively.

2.3. Catalytic reactions

2.3.1. Isomerization-esterification reaction

The conversion of 1, 3-dihydroxylacetone (DHA) to methyl lactate in the presence of methanol was carried out in a tightly closed glass vial. In a typical experiment, 2 mmol DHA in 5 mL methanol was mixed with 100 mg catalyst, then the mixture was stirred vigorously and heated at designated temperature for certain reaction time. At the end of the test, the catalyst was separated by centrifugation and the products were analyzed by a Shimadzu 2010 GC (Agilent HP-5MS column, 30 m × 0.25 mm × 0.25 μm; FID detector) with mesitylene as the internal standard. The products were identified by the gas chromatograph-mass spectrometry (GC-MS, Agilent 6890, HP-5 column and Agilent 5973 mass selective detector).

For the recycling tests, the used catalysts were washed with methanol for 3 times, dried at 80 °C for 12 h and calcined at 400 °C in flowing air for the next run.

2.3.2. Bayer-Villager oxidation

The Baeyer-Villiger oxidation of cyclopentanone was carried out in a 25 mL round-bottomed flask equipped with a refluxed condenser. In a typical experiment, 2 mmol cyclopentanone, 5 mL benzotrifluoride, and 0.5 mmol mesitylene (internal standard) were mixed in the flask, which was heated to the reaction temperature of 90 °C for 15 min and then 3 mmol H_2O_2 (50 wt%, H_2O_2/ketone = 1.5) was added to initiate the reaction. After reaction, the solid catalyst was separated by centrifugation and the liquid phase was quantified by a Shimadzu 2010 GC (Agilent HP-5 MS column, 30 m × 0.25 mm × 0.25 μm; FID detector).

2.3.3. Aldol condensation

The aldol condensation reaction between furfural and acetone was performed in a 15 mL stainless-steel autoclave. In the typical experiment, 1.25 mmol furfural, 12.5 mmol of acetone, 0.25 mmol mesitylene (internal standard), and 0.1 g zeolite catalyst were well mixed in the stainless-steel autoclave. Then, 1.0 Mpa N_2 was injected into the autoclave, which was subsequently sealed and rapidly heated to 120 °C under stirring. After reaction, the solid catalyst was separated by centrifugation and the liquid phase was analyzed by a Shimadzu 2010 GC (Agilent HP-5 MS column, 30 m × 0.25 mm × 0.25 μm; FID detector).

3. Results and discussion

3.1. Structural and compositional properties of Sn-MFI and Sn-Al-MFI zeolites

The crystalline phase of the calcined zeolite samples was first examined by X-ray diffraction. As showed in Fig. 1a, all samples show the typical and exclusive diffraction peaks corresponding to MFI topology, indicating the successful preparation of Sn-containing MFI zeolites via the in situ hydrothermal method. The as-prepared Sn-MFI zeolites appear as nanocrystals with size of ~100 nm (see Fig. S1 for typical SEM

Table 1
Physico-chemical properties of Sn-containing zeolites.

Sample	Sn Loading		Si/Al[a]	Si/Sn[a]	S_{BET} (m^2/g)	V_{micro} (m^3/g)	Relative Crystallinity
	Target	Actual[a]					
Silicate-1	0	0	> 2000	> 2000	542	0.196	100%
1.6% Sn-MFI	2.0	1.6	> 2000	122	480	0.172	84%
2.5% Sn-MFI	3.0	2.5	> 2000	77	471	0.166	82%
2.8% Sn-MFI	4.0	2.8	> 2000	69	450	0.160	73%
2.3% Sn-Al-MFI-240	3.0	2.3	240	86	427	0.153	80%
2.2% Sn-Al-MFI-160	3.0	2.2	160	90	422	0.140	76%
2.2% Sn-Al-MFI-80	3.0	2.2	80	90	356	0.102	75%

[a] Determined by ICP.

image of 2.5% Sn-MFI sample), and the introduction of Al species increases the crystal size to ~200 nm.

The structural information about these samples were further investigated by FTIR spectroscopy, and the results are shown in Fig. 1b. The distinct bands at 450, 550, 790 and 1105 cm^{-1} ascribable to the Si-O bending vibrations, pentasil framework vibrations, and Si-O-Si symmetric and asymmetric stretching vibrations [27,28], respectively, are clearly identified. In addition, the bands at ~960 cm^{-1}, which is commonly used as an indicator of Sn incorporation in the zeolite framework [29–31], are not observed in the present study. According to recent FTIR studies of Courtney et al. this band, which is proportional to the Sn concentration in the zeolite, could be due to the hydroxylated Si-OH groups or the tetrahedrally coordinated Sn(IV) sites [32]. In this context, the absence of the bands at ~960 cm^{-1} in our Sn-containing MFI zeolites may be due to their low concentration of Si-OH defects and/or framework Sn species (Table 1).

The structural information about Sn-containing MFI zeolites was completed by ^{29}Si and ^{27}Al MAS NMR spectroscopy. As shown in Fig. 2a, all zeolites exhibit a similar strong signal at −113 ppm due to the framework $Si[OSi]_4$ (Q_4) units and two weak signals at −116 and −105 ppm due to Q_4 and Q_3 ($Si[OSi]_3[OH]$ or $Si[OSi]_3[1Al]$) species, respectively [33]. For Sn-Al-MFI samples, dominating signals at 55 ppm due to tetrahedrally coordinated framework Al species are observed (Fig. 2b), which will accordingly create Brønsted acid sites in zeolites (vide infra). The N_2 adsorption-desorption isotherms of Sn-containing zeolite samples were measured and shown in Fig. 3. The sharp adsorption uptakes in the low relative pressure range ($P/P_0 < 0.1$) confirm the typical microporosity of the as-synthesized zeolite samples. The specific surface area and micropore volume decrease to some extent by the presence of Sn and/or Al species. Nevertheless, high surface area of > 350 m^2/g and micropore volume of > 0.10 cm^3/g indicate the high quality of these zeolite materials. The physico-chemical properties of Sn-containing zeolite samples are summarized in Table 1 for a direct view. Obviously, after the introduction of Sn species, the relative crystallinity of the Sn-MFI and Sn-Al-MFI decreased a bit as compared with Silicate-1 (Fig. 1a), which is responsible for the decrease in the specific area and microporous volumes of the Sn-

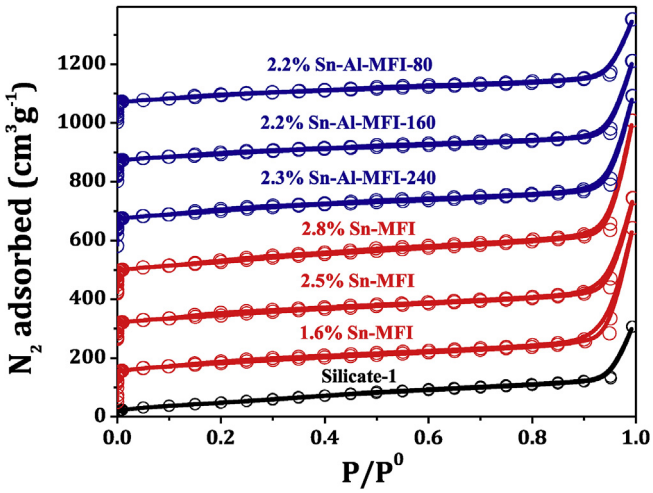

Fig. 3. N_2 absorption-desorption isotherms of silicate-1 and Sn-containing MFI zeolites.

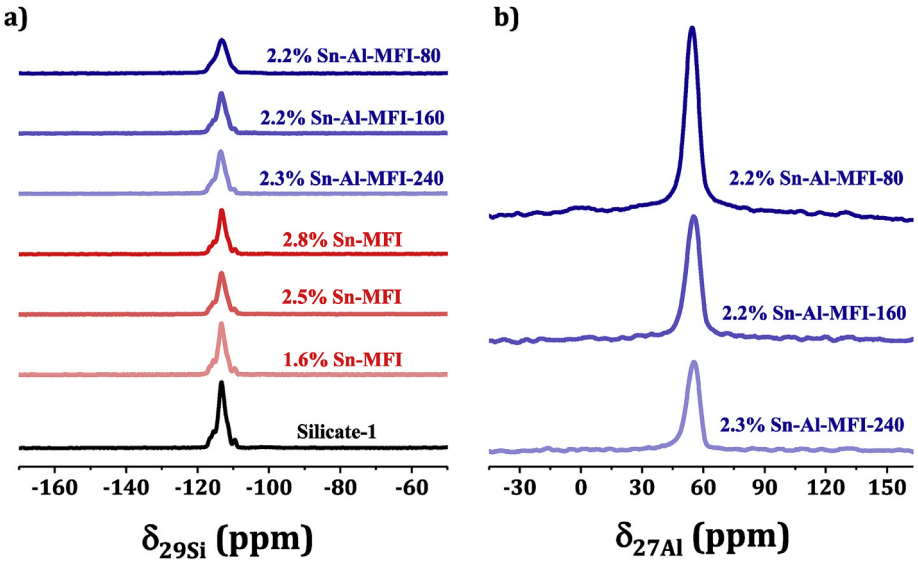

Fig. 2. (a) ^{29}Si MAS NMR of Sn-MFI and Sn-Al-MFI samples; (b) ^{27}Al MAS NMR of Sn-Al-MFI samples.

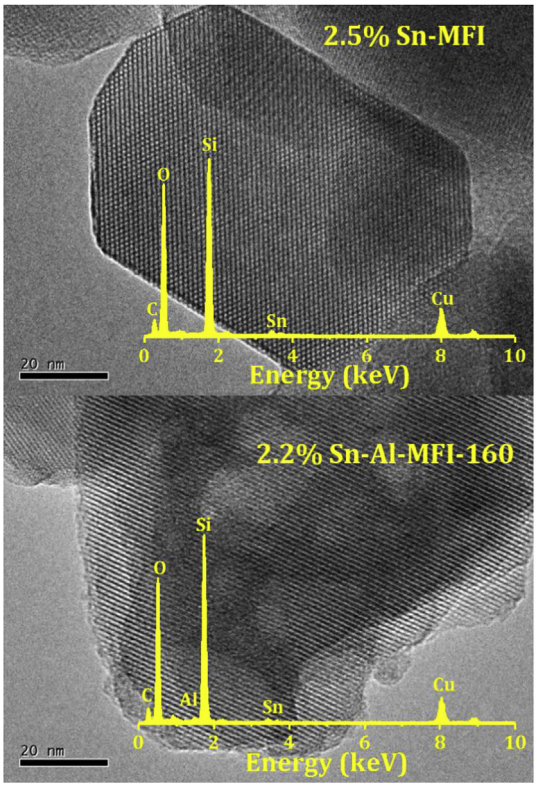

Fig. 4. HR-TEM images of 2.5% Sn-MFI and 2.2% Sn-Al-MFI-160 zeolites with EDS shown inset.

containing zeolites.

3.2. Coordination state of Sn species in Sn-MFI and Sn-Al-MFI zeolites

The dispersion of Sn species in Sn-containing MFI zeolite nanocrystals can be directly observed via HRTEM microscopy. As shown in Fig. 4, the pure single MFI crystals with clear lattice fringes can be clearly identified for 2.5% Sn-MFI and 2.2% Sn-Al-MFI-160. No Sn-containing aggregates are detected although the presence of > 2.0% Sn is revealed by EDS analysis (yellow spectrum inset). That is, Sn species are homogeneously distributed in 2.5% Sn-MFI, 2.2% Sn-Al-MFI-160 (Fig. 4) and other Sn-containing MFI zeolites (Fig. S2).

The existing states of Sn species in Sn-containing MFI zeolites were characterized by means of XPS. As shown in Fig. 5a, two binding energy values at 486.6 and 495.0 eV due to Sn $3d_{5/2}$ and $3d_{3/2}$ of octahedral Sn (IV) species are observed for reference SnO_2, while for the MFI zeolite supporting with small SnO_2 clusters, i.e. 2.6%SnO_2/MFI, the binding energy values shift a little bit to 487.3 and 495.7 eV, which are between the values of bulk SnO_2 and Sn-containing MFI zeolites. This could be due to the weak interaction between the SnO_2 and Silicatie-1. By comparison, two similar binding energy values at 487.6 and 496.0 eV due to Sn 3d5/2 and 3d3/2 of isolated tetrahedrally coordinated Sn(IV) species occur in all the Sn-containing samples [16–18], and which definitely excludes the presence of octahedral Sn(IV) species. In addition, the presence of framework Al species in the Sn-Al-MFI samples has no noticeable influence on binding energy values of Sn species. The XPS results reveal that Sn species in Sn-MFI samples are tetrahedrally coordinated in MFI framework.

UV-vis spectroscopy can provide information on the chemical environment of Sn species within the zeolite framework. For reference samples, i.e. bulk SnO_2 and SnO_2/MFI, a broad signal between 250 and 300 nm are observed (Fig. 5b), which are attributed to the charge transfer from Sn-O-Sn bands. The UV-vis spectra of Sn-containing MFI zeolite samples show similar adsorption bands centered at ~200 nm (Fig. 5b), indicative of the dominating tetra-coordinated Sn(IV) species [16,34,35]. The absence of an absorbance at > 250 nm definitely excludes the existence of octahedral Sn(IV) species from SnO_2 nanoparticles or even small clusters, which is in good agreement with the XPS results.

3.3. Acid properties of Sn-MFI and Sn-Al-MFI zeolites

The introduction of Sn and/or Al species to pure-silica MFI zeolite is expected to create acid sites, and the acidic properties of Sn-MFI and Sn-Al-MFI zeolites were evaluated by means of NH_3-TPD, FTIR spectroscopy of pyridine adsorption, and ^1H and ^{31}P MAS NMR spectroscopy after ammonia and TMPO adsorption.

NH_3-TPD is first employed to analyze the amount and strength of acid sites in the Sn-containing MFI samples. As shown in Fig. 6a, different amounts of acid sites with distinct strength are created from Sn species dispersed within MFI zeolites (ammonia desorption peaks at 100–500 °C). With Al incorporation into Sn-MFI structure, additional strong acid sites are created when compared with Al-free Sn-MFI. The types of acid sites in selected Sn-containing zeolites samples were determined by FTIR spectroscopy of pyridine adsorption (Fig. 6b). Generally, pyridine adsorption at the Lewis acid sites gives rise to the FTIR bands at 1450, 1490, and 1610 cm^{-1}, while pyridine adsorption at the Brønsted acid sites causes bands at 1490, 1550, and 1640 cm^{-1} [36–38]. As shown in Fig. 6b, Lewis acid sites (bands at 1450, 1490, and 1610 cm^{-1}) are detected for 2.5% Sn-MFI, while both Lewis and Brønsted acid sites (band at 1550 cm^{-1}) were detected for 2.2% Sn-Al-MFI-160.

The hydroxyl groups of 2.5% Sn-MFI and 2.2% Sn-Al-MFI-160 zeolites were analyzed by ^1H MAS NMR spectroscopy before and after ammonia adsorption. As shown in Fig. 7a, a dominant signal at δ_{1H} = 1.6 ppm due to silanol groups at framework defects occurs in these two samples. After ammonia loading, a strong increase of the signal intensities in the shift range of δ_{1H} = 0.8–3.0 ppm occurs on 2.5% Sn-MFI and 2.2% Sn-Al-MFI-160 zeolites. According to previous reports, these signals are due to ammonia molecules coordinated at Lewis acid sites [39,40]. In addition, a sharp signal at δ_{1H} = 6.4 ppm occurs for 2.2% Sn-Al-MFI-160 zeolite, which is attributed to a protonation of ammonia by accessible Brønsted acid sites [41]. This indicates that strong Brønsted acid sites were created after the Al incorporation into Sn-MFI structure.

To support the assignment of the nature of surface sites on the Sn-containing MFI zeolites under study, TMPO was also utilized as a probe molecule. The ^{31}P MAS NMR spectrum of the samples after TMPO loading are shown in Fig. 7b. According to previous reports, the signals occurring at 46–50 ppm in the spectra of 2.5% Sn-MFI and 2.2% Sn-Al-MFI-160 zeolites are attributed to TMPO adsorbed at Lewis acid sites [39]. Additional signals appearing at 56–61 ppm for 2.2% Sn-Al-MFI-160 zeolite are typical for TMPO interacting with Brønsted acid sites, which agrees well with the ^1H MAS NMR results (Fig. 7a). Additionally, two sharp signals at 41 and 27 ppm occur for 2.5% Sn-MFI and 2.2% Sn-Al-MFI-160 zeolites. The former one is due to the physisorbed TMPO at non-acidic silanol groups, while the latter one is likely due to “mobile” TMPO that either is attached in the intercrystalline voids or is weakly adsorbed near the opening of the channel pores of the zeolites [42].

The quantitative analysis of the acid sites of the samples from the ^1H MAS NMR spectra after ammonia loading is summarized in Table 2, and a comparable number of Lewis acid sites of 0.10 and 0.09 mmol/g could be obtained over 2.2% Sn-Al-MFI-160 and 2.5% Sn-MFI catalysts, respectively. Additionally, certain amount of Brønsted acid sites (0.06 mmol/g) is obtained over 2.2% Sn-Al-MFI-160 catalyst. This is in good agreement with the quantitative results from the FTIR spectra of pyridine adsorption, indicating that the Lewis acidic Sn-MFI and the bifunctional Sn-Al-MFI have been successfully prepared via the present direct hydrothermal strategy.

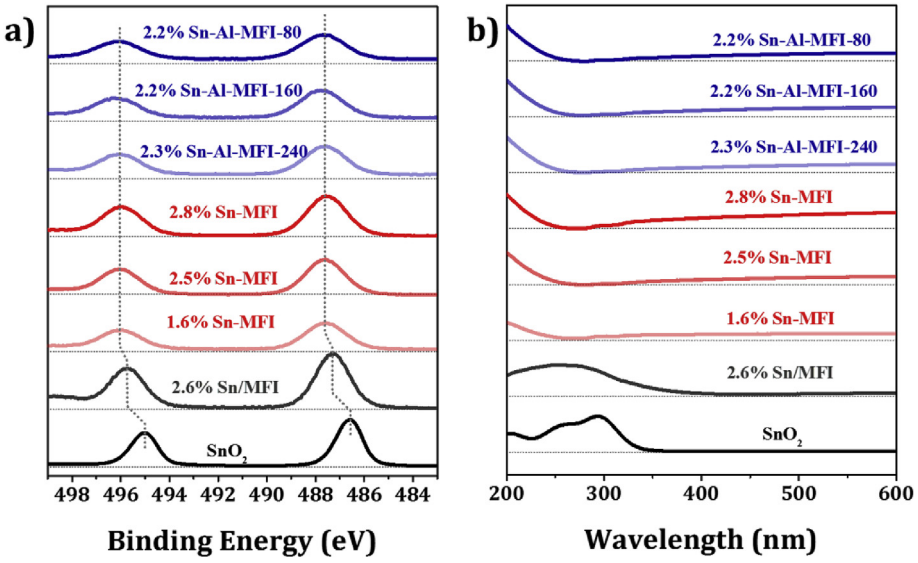

Fig. 5. (a) Sn 3d XPS of SnO_2, 2.6%Sn/MFI, Sn-MFI and Sn-Al-MFI zeolites; (b) UV-vis spectra of dehydrated SnO_2, 2.6%Sn/MFI, Sn-MFI and Sn-Al-MFI samples.

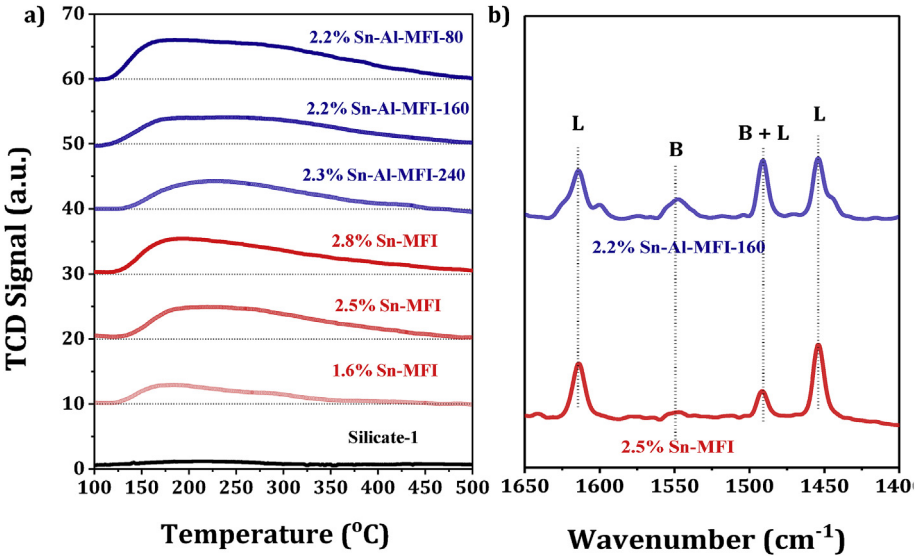

Fig. 6. (a) NH_3-TPD profiles of silicate-1 and Sn-containing MFI zeolites; (b) FTIR spectra of pyridine adsorption on 2.5% Sn-MFI and 2.2% Sn-Al-MFI-160.

3.4. Catalytic properties of Sn-MFI in various reactions

The catalytic activity of the as-prepared Sn-containing catalysts, including Sn-MFI and Sn-Al-MFI, was first investigated in the isomerization-esterification reaction of DHA in methanol. The reaction network has been studied intensively [13,38,43], and there is a general agreement that DHA, in fast equilibrium with its isomer glyceraldehyde (GA), undergoes dehydration and rearrangement into pyruvic aldehyde (PAL) (Scheme 1). This reaction can be catalyzed by Lewis acid or Brønsted acid sites. With the presence of few Brønsted acid sites, the initial dehydration step for producing PA from DHA or GLA can be greatly promoted, while too much Brønsted acid sites could further catalyze the formed PA to PADA, which would be discussed in the following parts.

As it is shown in Table S1, good catalytic activity with a DHA conversion of 100% could be achieved both over Sn-MFI and Sn-Al-MFI catalysts under certain conditions. Obviously, 2.2% Sn-Al-MFI-160 showed a faster formation of ML in comparison with Al-free 2.5% Sn-MFI with the comparable Sn content (Fig. 8). This behavior is due to a more efficient conversion of DHA, caused by a fast Brønsted acid-catalyzed dehydration reaction [13,20,38], which can by supported by the lower apparent activation energy of 2.2% Sn-Al-MFI-160 (47.6 kJ/mol) than that of 2.5% Sn-MFI (64.9 kJ/mol) (Fig. 9a). Additionally, the presence of Brønsted acid sites in 2.2% Sn-Al-MFI-160 can also cause the further conversion of PA to PADA (Scheme 1), and therefore, results in a little decrease in the selectivity to ML (~95%) in comparison with 2.5% Sn-MFI (99%). With increasing Al contents in the Sn-MFI catalysts, the selectivity to ML decreases slightly to 88.6% (Table S1), while the selectivity to pyruvic aldehyde methyl hemiacetal (PADH) increases instead. It indicates that more Brønsted acid sites are unfavorable for the ML formation, and the PAMH intermediates can be further converted to PADH (Scheme 1). Therefore, 2.2% Sn-Al-MFI-160 catalyst with appropriate amounts of Brønsted and Lewis acid sites exhibits the highest methyl lactate productivity, and which is comparable with the literature results (Table S3).

To verify the recycling abilities of the Sn-containing MFI zeolite

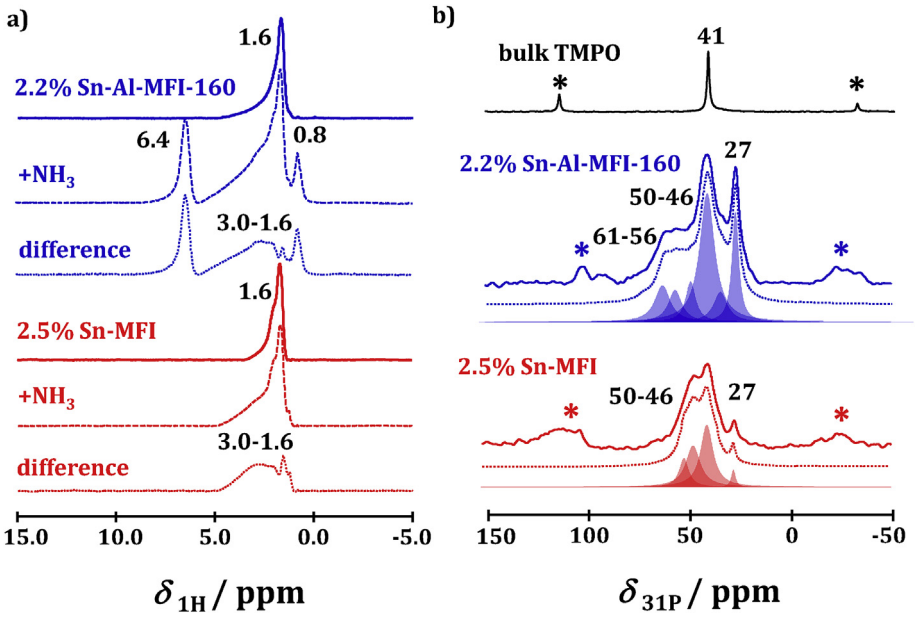

Fig. 7. (a) ^{1}H MAS NMR spectroscopy of ammonia adsorption on 2.5% Sn-MFI and 2.2% Sn-Al-MFI-160 zeolites; (b) ^{31}P MAS NMR spectroscopy of TMPO adsorption on 2.5% Sn-MFI and 2.2% Sn-Al-MFI-160 zeolites.

Table 2
^{1}H and ^{31}P MAS NMR investigations of the surface acid sites on 2.2% Sn-Al-MFI-160, and 2.5% Sn-MFI by using trimethylphosphine oxide (TMPO) and ammonia as probe molecules.

Catalysts	^{1}H MAS NMR	^{31}P MAS NMR
2.2% Sn-Al-MFI-160	**Signal at 0.8–3.0 ppm:** NH_3 at Lewis acid sites (0.10 mmol/g)[a] **Signal at 6.4 ppm:** NH_4^+ at Brønsted acid sites (0.06 mmol/g)[a]	**Signal at 46–50 ppm:** TMPO at Lewis acid sites **Signal at 56–61 ppm:** TMPO at Brønsted acid sites
2.5% Sn-MFI	**Signal at 0.8–3.0 ppm:** NH_3 at Lewis acid sites (0.09 mmol/g)[a] **Signal at 6.4 ppm:** none	**Signal at 46–50 ppm:** TMPO at Lewis acid sites **Signal at 56–61 ppm:** none

[a] Experimental accuracy: ± 10%.

catalysts, five consecutive reaction cycles were performed with the 2.5% Sn-MFI and 2.2% Sn-Al-MFI-160 catalysts (Fig. 9b). After washing, drying, and calcination of the used catalysts, the catalytic activity of the regenerated materials could be fully recovered, and no

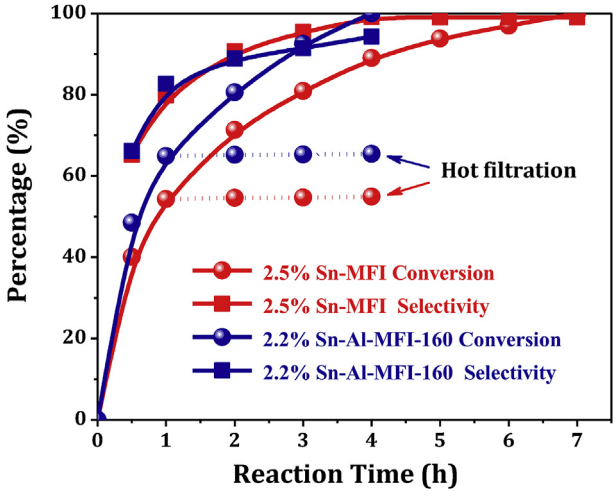

Fig. 8. Catalytic properties of Sn-containing zeolites in triose isomerization. Time-dependent dihydroxylacetone conversion to methyl lactate catalyzed by 2.5% Sn-MFI and 2.2% Sn-Al-MFI-160 at 90 °C (hot filtration results shown inset). Reaction conditions: Dihydroxylacetone 2 mmol, CH_3OH 5 mL, catalyst 100 mg.

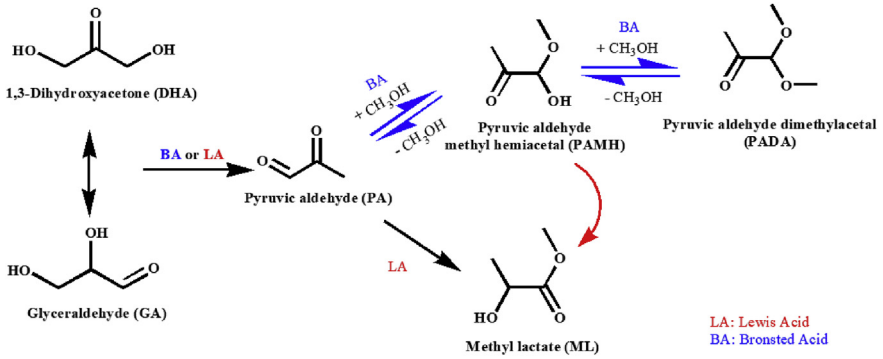

Scheme 1. Reaction route of the dihydroxyacetone conversion to methyl lactate. The acid sites needed for each step are also displayed in the route. Brønsted acid sites (BA) are marked in blue, while Lewis acid sites (LA) are marked in red.

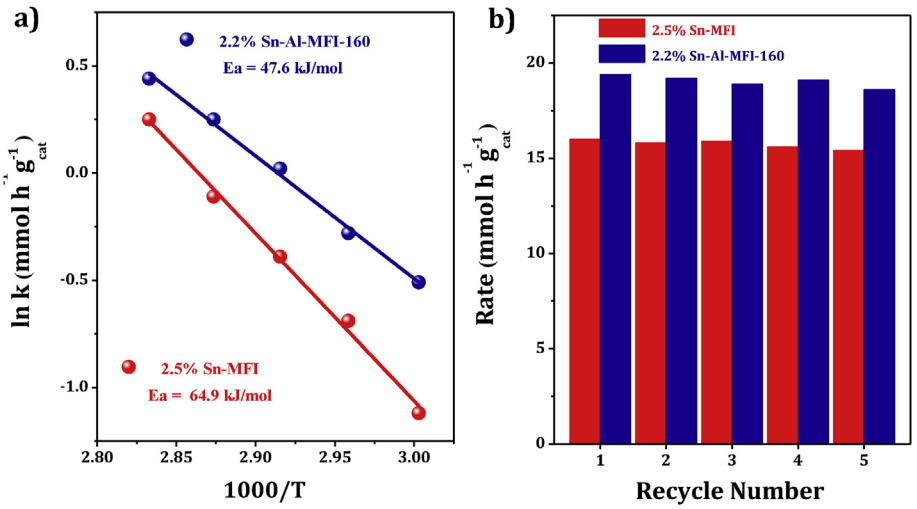

Fig. 9. (a) Kinetic plots of dihydroxylacetone conversion over 2.5% Sn-MFI and 2.2% Sn-Al-MFI-160 zeolites; Reaction conditions: Dihydroxylacetone 2 mmol, CH_3OH 5 mL, catalyst 40 mg. (b) Recycling test of 2.5% Sn-MFI and 2.2% Sn-Al-MFI-160 in dihydroxylacetone conversion to methyl lactate at 90 °C. Reaction conditions: Dihydroxylacetone 2 mmol, CH_3OH 5 mL, catalyst 100 mg.

significant changes in their catalytic activity were observed for upon five cycles, which demonstrates their high potential for future applications. This regeneration test is in line with the result of the hot filtration test (Fig. 8). Hot-filtration based leaching test was performed to determine whether the tetrahedrally coordinated Sn(IV) species could leach from the catalyst into the reaction solutions and probably participate the reaction process. The 2.5% Sn-MFI and 2.2% Sn-Al-MFI-160 catalysts were removed from the reaction mixture by centrifugation after the reaction time of 1 h, and the filtrates proceeded by themselves for another 3 h under the same reaction conditions. As shown in Fig. 8, the removal of the catalyst led to complete termination of the reaction, confirming the heterogeneous nature of the Sn-containing MFI catalyst in the DHA conversion.

The 2.2% Sn-Al-MFI-160 and 2.5% Sn-MFI catalysts also exhibit considerable activity in the condensation reaction between furfural and acetone, confirming that they are reliable solid Lewis acid catalysts (Fig. 10a). Furthermore, 2.2% Sn-Al-MFI-160 exhibits distinctly higher activity than 2.5% Sn-MFI in the Baeyer-Villiger oxidation of cyclopentanone (Fig. 10b), revealing the synergistic effect between Brønsted and Lewis acid sites and its unexpected beneficial effect in Baeyer-Villiger oxidation reaction. This phenomenon could be caused by Brønsted acid sites, which facilitate the hydrolysis of lactate products. These products are formed in the Baeyer-Villiger reaction process. The generated carboxylic acid behave as a homogeneous catalyst and is responsible for the marvellous catalytic effects in the oxidation process [44,45].

4. Conclusion

In summary, a facile and scalable strategy has been established to obtain the Sn-containing MFI zeolites with the controllable Al contents. The key point of this strategy is that citrate is firstly employed as buffer solution to construct the EDTA-Sn complex as tin source, and then Na_2CO_3 is utilized to adjust the complex solution to neutral for ease of use. In addition to the Lewis acidic Sn(IV) sites, the Brønsted acidic Al (III) sites could also be introduced into the MFI framework simultaneously. Both the Sn-MFI and Sn-Al-MFI zeolite catalysts exhibited the remarkable catalytic performance in the conversion of DHA to ML, while the combination effects of the Brønsted and Lewis acid sites in Sn-Al-MFI catalyst could significantly promote its activity. The as-prepared Sn-MFI zeolites also exhibited appreciable catalytic activity in the aldol condensation and Bayer-Villager oxidation reaction, revealing the nature of their versatile catalytic properties. The direct hydrothermal synthesis route can be potentially developed into a general strategy to prepare heteroatom-containing zeolites for solid acid catalysis and other related materials.

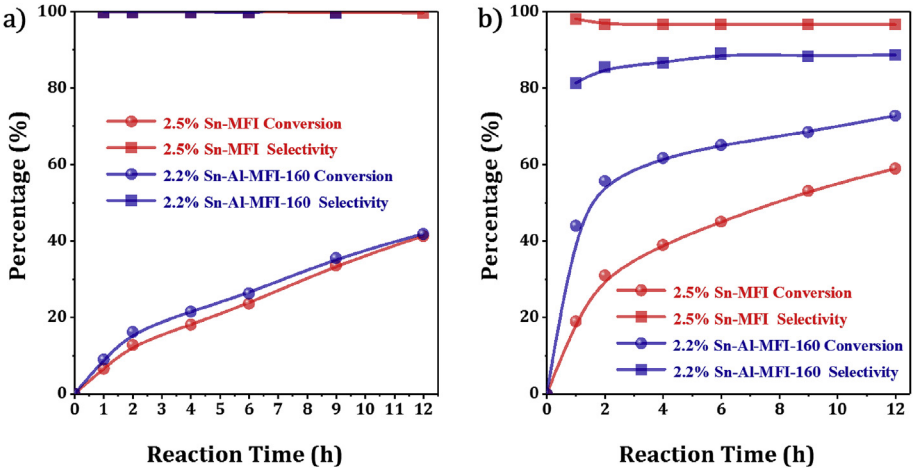

Fig. 10. (a) The Baeyer-Villiger oxidation of cyclopentanone over 2.5% Sn-MFI and 2.2% Sn-Al-MFI-160 catalysts. Reaction conditions: 2 mmol cyclopentanone, 3 mmol hydrogen peroxide (50 wt %), 5 mL benzotrifluoride, catalyst 100 mg, 90 °C; (b) The aldol condensation reaction between furfural and acetone over 2.5% Sn-MFI and 2.2% Sn-Al-MFI-160 catalysts. Reactions conditions: 1.25 mmol furfural, 12.5 mmol acetone, 100 mg catalyst, 120 °C, under N_2 pressure (1.0 MPa).

Acknowledgements

This work is supported by the National Natural Science Foundation of China (21573113, 21722303, and 21421001), Municipal Natural Science Foundation of Tianjin (16JCQNJC04900), 111 project (B18030), Sinopec Corp. (417012-2) and the Foundation of China Scholarship Council (CSC).

Appendix A. Supplementary data

Supplementary data related to this article can be found at http://dx.doi.org/10.1016/j.micromeso.2018.05.032.

References

[1] A. Corma, S. Iborra, A. Velty, Chemical routes for the transformation of biomass into chemicals, Chem. Rev. 107 (2007) 2411–2502.
[2] S. Tolborg, S. Meier, I. Sádaba, S.G. Elliot, S.K. Kristensen, S. Saravanamurugan, A. Riisager, P. Fristrup, T. Skrydstrup, E. Taarning, Tin-containing silicates: identification of a glycolytic pathway via 3-deoxyglucosone, Green Chem. 18 (2016) 3360–3369.
[3] M. Moreno-Recio, J. Santamaria-Gonzalez, P. Maireles-Torres, Brönsted and Lewis acid ZSM-5 zeolites for the catalytic dehydration of glucose into 5-hydroxymethylfurfural, Chem. Eng. J. 303 (2016) 22–30.
[4] L. Nemeth, S.R. Bare, Science and technology of framework metal-containing zeotype catalysts, Adv. Catal. 57 (2014) 1–97.
[5] M. Morales, P.Y. Dapsens, I. Giovinazzo, J. Witte, C. Mondelli, S. Papadokonstantakis, K. Hungerbuhler, J. Perez-Ramirez, Environmental and economic assessment of lactic acid production from glycerol using cascade bio and chemocatalysis, Energy Environ. Sci. 8 (2015) 558–567.
[6] A. Corma, M.E. Domine, L. Nemeth, S. Valencia, Al-Free Sn-Beta zeolite as a catalyst for the selective reduction of carbonyl compounds (Meerwein-Ponndorf-Verley Reaction), J. Am. Chem. Soc. 124 (2002) 3194–3195.
[7] Z.H. Kang, X.F. Zhang, H.O. Liu, J.S. Qiu, K.L. Yeung, A rapid synthesis route for Sn-Beta zeolites by steam-assisted conversion and their catalytic performance in Baeyer-Villiger oxidation, Chem. Eng. J. 218 (2013) 425–432.
[8] P.Y. Dapsens, C. Mondelli, J. Perez-Ramirez, Design of Lewis-acid centres in zeolitic matrices for the conversion of renewables, Chem. Soc. Rev. 44 (2015) 7025–7043.
[9] Y. Roman-Leshkov, M.E. Davis, Activation of carbonyl-containing molecules with solid Lewis acids in aqueous media, ACS Catal. 1 (2011) 1566–1580.
[10] T. Ennaert, J.V. Aelst, J. Dijkmans, R.D. Clercq, W. Schutyser, M. Dusselier, D. Verboekend, B.F. Sels, Potential and challenges of zeolite chemistry in the catalytic conversion of biomass, Chem. Soc. Rev. 45 (2016) 584–611.
[11] M. Moliner, Y. Román-Leshkov, M.E. Davis, Tin-containing zeolites are highly active catalysts for the isomerization of glucose in water, Proc. Natl. Acad. Sci. Unit. States Am. 107 (2010) 6164–6168.
[12] L. Li, C. Stroobants, K.F. Lin, P.A. Jacobs, B.F. Sels, P.P. Pescarmona, Selective conversion of trioses to lactates over Lewis acid heterogeneous catalysts, Green Chem. 13 (2011) 1175–1181.
[13] P.P. Pescarmona, K.P.F. Janssen, C. Delaet, C. Stroobants, K. Houthoofd, A. Philippaerts, C.D. Jonghe, J.S. Paul, P.A. Jacobs, B.F. Sels, Zeolite-catalysed conversion of C_3 sugars to alkyl lactates, Green Chem. 12 (2010) 1083–1089.
[14] J. Dijkmans, M. Dusselier, D. Gabriels, K. Houthoofd, P.C.M.M. Magusin, S.G. Huang, Y. Pontikes, M. Trekels, A. Vantomme, L. Giebeler, S. Oswald, B.F. Sels, Cooperative catalysis for multistep biomass conversion with Sn/Al Beta zeolite, ACS Catal. 5 (2015) 928–940.
[15] L. Li, X. Collard, A. Bertrand, B.F. Sels, P.P. Pescarmona, C. Aprile, Extra-small porous Sn-silicate nanoparticles as catalysts for the synthesis of lactates, J. Catal. 314 (2014) 56–65.
[16] E. Taarning, S. Saravanamurugan, M.S. Holm, J.M. Xiong, R.M. West, C.H. Christensen, Zeolite-catalyzed isomerization of triose sugars, ChemSusChem 2 (2009) 625–627.
[17] M. Moliner, State of the art of Lewis acid-containing zeolites: lessons from fine chemistry to new biomass transformation processes, Dalton Trans. 43 (2014) 4197–4208.
[18] W.N.P. van der Graaff, G.N. Li, B. Mezari, E.A. Pidko, E.J.M. Hensen, Synthesis of Sn-Beta with exclusive and high framework Sn content, ChemCatChem 7 (2015) 1152–1160.
[19] A. Corma, L.T. Nemeth, M. Renz, S. Valencia, Sn-zeolite Beta as a heterogeneous chemoselective catalyst for Baeyer-Villiger oxidations, Nature 412 (2001) 423–425.
[20] C. Hammond, S. Conrad, I. Hermans, Simple and scalable preparation of highly active Lewis acidic Sn-β, Angew. Chem. Int. Ed. 51 (2012) 11736–11739.
[21] J. Dijkmans, J. Demol, K. Houthoofd, S.G. Huang, Y. Pontikes, B.F. Sels, Post-synthesis Sn-β: an exploration of synthesis parameters and catalysis, J. Catal. 330 (2015) 545–557.
[22] N.K. Mal, V. Ramaswamy, P.R. Rajamohanan, A.V. Ramaswamy, Sn-MFI molecular sieves: synthesis methods, ^{29}Si liquid and solid MAS-NMR, ^{119}Sn static and MAS NMR studies, Microporous Mater. 12 (1997) 331–340.
[23] N.G. Vargas, S. Stevenson, D.F. Shantz, Synthesis and characterization of tin(IV) MFI: sodium inhibits the synthesis of phase pure materials, Microporous Mesoporous Mater. 152 (2012) 37–49.
[24] P.S. Niphadkar, N.P. Tangale, P.N. Joshi, S.V. Awate, Crystallization kinetics of Sn-MFI molecular sieve formation by dry gel conversion method, Microporous Mesoporous Mater. 182 (2013) 73–80.
[25] F. Fringuelli, F. Pizzo, L. Vaccaro, Lewis-acid catalyzed organic reactions in water. The case of $AlCl_3$, $TiCl_4$, and $SnCl_4$ believed to be unusable in aqueous medium, J. Org. Chem. 66 (2001) 4719–4722.
[26] C.V.G. Reddy, S.V. Manorama, V.J. Rao, Preparation and characterization of barium stannate: application as a liquefied petroleum gas sensor, J. Mater. Sci. Mater. Electron. 12 (2001) 137–142.
[27] Y.T. Meng, H.C. Genuino, C.H. Kuo, H. Huang, S.Y. Chen, L.C. Zhang, A. Rossi, S.L. Suib, One-step hydrothermal synthesis of manganese-containing MFI-type zeolite, Mn-ZSM-5, characterization, and catalytic oxidation of hydrocarbons, J. Am. Chem. Soc. 135 (2013) 8594–8605.
[28] G. Vitale, H. Molero, E. Hernandez, S. Aquino, V. Birss, P. Pereira-Almao, One-pot preparation and characterization of bifunctional Ni-containing ZSM-5 catalysts, Appl. Catal. Gen. 452 (2013) 75–87.
[29] N.K. Mal, A.V. Ramaswamy, Synthesis and catalytic properties of large-pore Sn-β and Al-free Sn-β molecular sieves, Chem. Commun. (1997) 425–426.
[30] K. Chaudhari, T.K. Das, P.R. Rajmohanan, K. Lazar, S. Sivasanker, A.J. Chandwadkar, Synthesis, characterization, and catalytic properties of mesoporous Tin-containing analogs of MCM-41, J. Catal. 183 (1999) 281–291.
[31] Z.H. Kang, X.F. Zhang, H.O. Liu, J.S. Qiu, W. Han, K.L. Yeung, Factors affecting the formation of Sn-Beta zeolites by steam-assisted conversion method, Mater. Chem. Phys. 141 (2013) 519–529.
[32] T.D. Courtney, C.C. Chang, R.J. Gorte, R.F. Lobo, W. Fan, V. Nikolakis, Effect of water treatment on Sn-BEA zeolite: origin of 960 cm^{-1} FTIR peak, Microporous Mesoporous Mater. 210 (2015) 69–76.
[33] B. Tang, W.L. Dai, X.M. Sun, N.J. Guan, L.D. Li, M. Hunger, A procedure for the preparation of Ti-Beta zeolites for catalytic epoxidation with hydrogen peroxide, Green Chem. 16 (2014) 2281–2291.
[34] E.V. Beletskiy, X.L. Hou, Z.L. Shen, J.R. Gallagher, J.T. Miller, Y.Y. Wu, T.H. Li, M.C. Kung, H.H. Kung, Supported tetrahedral oxo-Sn catalyst: single site, two modes of catalysis, J. Am. Chem. Soc. 138 (2016) 4294–4297.
[35] H.Y. Luo, L. Bui, W.R. Gunther, E. Min, Y. Roman-Leshkov, Synthesis and catalytic activity of Sn-MFI nanosheets for the Baeyer-Villiger oxidation of cyclic ketones, ACS Catal. 2 (2012) 2695–2699.
[36] R. Buzzoni, S. Bordiga, G. Ricchiardi, C. Lamberti, A. Zecchina, G. Bellussi, Interaction of pyridine with acidic (H-ZSM-5, H-β, H-Mode zeolites) and superacidic (H-Nafion membrane) systems: an IR investigation, Langmuir 12 (1996) 930–940.
[37] P. Li, G.Q. Liu, H.H. Wu, Y.M. Liu, J.G. Jiang, P. Wu, Postsynthesis and selective oxidation properties of nanosized Sn-Beta zeolite, J. Phys. Chem. B 115 (2011) 3663–3670.
[38] H.J. Cho, P. Dornath, W. Fan, Synthesis of hierarchical Sn-MFI as Lewis acid catalysts for isomerization of cellulosic sugars, ACS Catal. 4 (2014) 2029–2037.
[39] S. Lang, M. Benz, U. Obenaus, R. Himmelmann, M. Hunger, Novel approach for the characterization of Lewis acidic solid catalysts by solid-state NMR spectroscopy, ChemCatChem 8 (2016) 2031–2036.
[40] T. Yan, W. Dai, G. Wu, S. Lang, M. Hunger, N. Guan, L. Li, Mechanistic insights into one-step catalytic conversion of ethanol to butadiene over bifunctional Zn-Y/Beta zeolite, ACS Catal. 8 (2018) 2760–2773.
[41] W. Dai, M. Scheibe, N. Guan, L. Li, M. Hunger, Fate of Brønsted acid sites and benzene-based carbenium ions during methanol-to-olefin conversion on SAPO-34, ChemCatChem 3 (2011) 1130–1133.
[42] Q. Zhao, W. Chen, S. Huang, Y.C. Wu, H.-K. Lee, S.-B. Liu, Discernment and quantification of internal and external acid sites on zeolites, J. Phys. Chem. B 106 (2002) 4462–4469.
[43] F. Clippel, M. Dusselier, R.V. Rompaey, P. Vanelderen, J. Dijkmans, E. Makshina, L. Giebeler, S. Oswald, G.V. Baron, J.F.M. Denayer, P.P. Pescarmona, P.A. Jacobs, B.F. Sels, Fast and selective sugar conversion to alkyl lactate and lactic acid with bifunctional carbon-silica catalysts, J. Am. Chem. Soc. 134 (2012) 10089–10101.
[44] Z.G. Zhu, H. Xu, J.G. Jiang, P. Wu, Postsynthesis and effective Baeyer-Villiger oxidation properties of hierarchical FAU-type stannosilicate, J. Phys. Chem. C 120 (2016) 23613–23624.
[45] G. Peris, S.J. Miller, A nonenzymatic acid/peracid catalytic cycle for the Baeyer-Villiger oxidation, Org. Lett. 10 (2008) 3049–3052.